Desalination and Water Treatment
www.deswater.com

doi: 10.5004/dwt.2020.24906

175 (2020) 282–292
January

A comparative study of the removal of cationic and anionic dyes from aqueous solutions using biochar as an adsorbent

Samiyappan Nirmaladevi*, Nachimuthu Palanisamy

Centre for Environmental Research, Department of Chemistry, Kongu Engineering College, Perundurai, Erode-638 060, Tamil Nadu, India, Tel. +91 9486636176; email: devinks86@gmail.com (S. Nirmaladevi), Tel. +91 9750264390; email: asppavithran@gmail.com (N. Palanisamy)

Received 17 May 2019; Accepted 12 September 2019

ABSTRACT

In the present study, *Acacia leucophloea* wood sawdust is utilized to prepare biochar by direct pyrolysis. This biochar is applied as an alternative adsorbent for the adsorption of Basic Red 29 (BR29) cationic dye and Reactive Red 2 (RR2) anionic dye. The adsorption performance of biochar on both the dyes is evaluated by varying the solution pH (2–10), agitation speed (30–170 rpm), initial dye concentration (40–100 mg L^{-1}), contact time (100 min), temperature (300, 310 and 320 K) and adsorbent dose (25–200 mg). The maximum removal of 98% is achieved for RR2 using biochar under the optimum conditions of 50 mg dosage, the temperature of 300 K, 170 rpm of agitation speed, 60 mg L^{-1} of initial dye concentration and pH of 2. For BR29, the same removal efficiency is achieved at pH 10 under the same operating conditions. The adsorption kinetics of both the dyes follows the pseudo-second-order model and the adsorption isotherms are best suited by the Freundlich model. Thermodynamic studies suggest that the adsorption process is spontaneous and exothermic for anionic dye and endothermic for cationic dye. These findings reveal that the biochar can be used as an alternative adsorbent to remove dyes from aqueous solutions.

Keywords: Reactive Red 2 (RR2); Basic Red 29 (BR29); Biochar; Adsorption; Kinetics

1. Introduction

Synthetic dyes have been used widely in many fields such as textiles, paper, leather tanning, plastics, rubber, and dye manufacturing industries [1,2]. Based on their charge upon dissolution in an aqueous medium, dyes can be classified as cationic (basic dyes), anionic (direct, acid and reactive dyes) and non-ionic (disperse dyes) [3]. Basic and reactive dyes have been used mostly in the textile industry because of their bright color, water-solubility, low cost and feasibility of application to fabric [4].

As they have a high intensity of colors, basic dyes are greatly visible even in very low concentrations. Reactive dyes are highly soluble in water and 5%–10% of the dyes released as such in the dye bath cause highly colored effluent polluting severely the environment [5]. Moreover, due to relative chemical stability and little biodegradability, the elimination of reactive dyes from the environment is a topic of much concern.

It has been reported that approximately 100 tons of dyes per year are discharged into water streams by the textile industries [6]. Hence the release of dyes into the environment creates environmental degradation. In an aqueous environment, dyes can cause skin allergies, cancer, mutation, reduced light penetration and reduced photosynthetic activity [7]. Therefore, it is necessary to apply efficient and effective techniques for the treatment of dyes to safeguard the environment.

Numerous methods such as adsorption, electro-coagulation, ion exchange, advanced oxidation process, biological

* Corresponding author.

treatment, and photocatalytic degradation have been applied to the treatment of dyes containing effluents [8]. Among these, adsorption is the most effective process used by the industries to remove the toxic chemicals present in the effluent. Various adsorbents such as clays [9,10], activated carbons in different forms [11], carbon nanotubes and nanocomposites [12,13] are used successfully to remove dyes from aqueous solution. The most widely used adsorbent for the adsorption process in industrial wastewater treatment systems is activated carbon due to its large specific surface area. However, activated carbon is more expensive and therefore its widespread use is restricted. Hence it is essential to search for low cost and easily available material as an alternative for activated carbon.

Thermal or hydrothermal degradation of biomass at elevated temperature with little or no oxygen yields a stable carbon-rich material referred to as biochar [14]. Biochar can be used as a sustainable sorbent to remove organic and inorganic pollutants from water [15]. Some studies have reported the utilization of biochar as an alternative adsorbent [16,17]. In the present study, batch mode adsorption experiments are conducted to study the adsorption ability of *Acacia leucophloea* wood sawdust (ALWSD) derived biochar for the removal of Basic Red 29 (BR29) and Reactive Red 2 (RR2) in aqueous solutions. To the best of knowledge, the current study is the first reported one to prepare biochar from ALWSD for dye removal via direct pyrolysis without any further activation process.

2. Materials and methods

2.1. Preparation and characterization of biochar

The precursor, whitebark ALWSD is collected from sawmills in the southern part of India. The samples are washed with water several times to remove the impurities, dried in sunlight, labeled as ALWSD and stored in a plastic container for the preparation of biochar. The biochar is prepared from ALWSD via the direct pyrolysis process. Approximately, 30 g of ALWSD is taken in a silica crucible covered with a lid and heated in a muffle furnace at a rate of 10°C min^{-1} until 700°C and held at this temperature for 2 h and allowed to cool at room temperature. The biochar produced is washed with distilled water and dried at 100°C. The dried biochar is ground with mortar and pestle and stored in a container for characterization and adsorption studies.

To elucidate the functional groups present in biochar before and after dyes adsorption, Fourier-transform infrared spectroscopy (FTIR) (PerkinElmer, USA) are recorded between 4,000 and 400 cm^{-1}. The crystalline phase of ALWSD and biochar is investigated by X-ray diffraction (XRD) measurements performed on an X'PERT-PRO diffractometer, (Netherlands), using monochromatic copper radiation at 45 kV and 30 mA over the 2θ range of 0°–80°. Further, the surface morphology of biochar before and after adsorption is analyzed by field emission-scanning electron microscopy (FE-SEM) (TESCAN performance in nanospace, USA) and the textural property is measured by N_2 adsorption–desorption isotherms at 77 K (Autosorb-1, Quantachrome). The carbon, hydrogen and nitrogen contents of biochar are determined with an elemental analyzer (Elementar Vario EL III). Further, the point of zero charges (pH_{pzc}) of the biochar is determined by salt addition method in a series of 100 mL conical flask using 0.1 mol L^{-1} KNO_3 solutions [18].

2.2. Adsorbate

The dyes selected for adsorption studies are RR2 with chemical formula $C_{19}H_{10}Cl_2N_6Na_2O_7S_2$, molecular weight = 615.34 g mol^{-1} and λ_{max} = 489 nm and BR29 with chemical formula of $C_{19}H_{17}ClN_4S$, molecular weight = 368.883 g mol^{-1} and λ_{max} = 476 nm purchased from local dye suppliers. To prepare the stock solution of 1,000 mg L^{-1}, the required amount of the dyes is dissolved in distilled water and the desired concentrations are obtained by further diluting the stock solution.

2.3. Batch adsorption experiments

The adsorption experiments are conducted in a series of 100 mL Erlenmeyer flasks containing 50 mL of the dye solutions and the flasks are agitated in an orbital shaker (REMI, RIS-24BL, Mumbai). Batch mode adsorption experiments are conducted by varying different parameters such as adsorbent dosage (25–200 mg), effect of pH (2–10), agitation speed (30–170 rpm), initial dye concentrations (40–100 mg L^{-1}) and contact time (100 min) to determine the optimum conditions for adsorption. The pH of the dye solutions is adjusted by using 0.1 M HCl or NaOH. Moreover, thermodynamic studies are conducted under the same procedure by varying solution temperatures (300, 310, and 320 K) keeping the other parameters constant. After all the studies, the adsorbent is separated by filtration and the dye concentration is determined by a UV-Visible spectrophotometer (Elico: DR3900, Hyderabad) using absorbance wavelength values (λ_{max}) for each dye. The percentage of dye removal, adsorption capacity (q_t, mg g^{-1}) and the equilibrium adsorption capacity (q_e, mg g^{-1}), is calculated by Eqs. (1)–(3), respectively.

$$\%\ \text{removal} = \left(\frac{C_0 - C_e}{C_0}\right) \times 100 \tag{1}$$

$$q_t = \frac{V(C_0 - C_t)}{m} \tag{2}$$

$$q_e = \frac{V(C_0 - C_e)}{m} \tag{3}$$

where V is the solution volume (L), m is the mass of adsorbent (g) and C_0, C_t and C_e are the dye concentrations (mg L^{-1}) at initial, at any time and equilibrium respectively.

The adsorption kinetics of RR2 and BR29 onto biochar is studied using pseudo-first-order in Eq. (4) [19] pseudo-second-order in Eq. (5) [20] and intra-particle diffusion models in Eq. (6) [21].

$$\log\left(q_e - q_t\right) = -\frac{K_1}{2.303}t + \log\left(q_e\right) \tag{4}$$

$$\frac{t}{q_t} = \left(\frac{1}{q_t}\right)t + \frac{1}{q_e^2 k_2} \tag{5}$$

$$q = k_p t^{0.5} + C \tag{6}$$

where k_1, k_2, and k_p are the pseudo-first-order (min^{-1}), pseudo-second-order (g mg^{-1} min^{-1}) and intra-particle diffusion rate constant (mg g^{-1} $min^{-1/2}$) respectively. C is a constant and it gives information about the thickness of the boundary layer.

Furthermore, the adsorption isotherms are studied using the Langmuir Eq. (7) [22], Freundlich Eq. (8) [23] and Temkin Eq. (9) [24] isotherm models.

$$\frac{C_e}{a_e} = \left(\frac{1}{Q^0_{\max}}\right) C_e + \frac{1}{Q^0_{\max} K_L} \tag{7}$$

$$\log q_e = \frac{1}{n} \log C_e + \log K_F \tag{8}$$

$$q_e = B \ln K_T + B \ln C_e \tag{9}$$

where $Q^0_{\max}$ (mg g^{-1}) is the maximum saturated monolayer adsorption capacity of an adsorbent, K_L (L mg^{-1}) is the Langmuir constant, K_F (mg g^{-1})(L mg^{-1})$^{-1/n}$ is the Freundlich's constant, n is the measure of the effectiveness of adsorption process, $B = R_T/b_T$ is the Temkin constant (J mol^{-1}) and K_T is the equilibrium binding constant corresponding to the maximum binding energy (L mg^{-1}).

Thermodynamic parameters of the adsorption process such as standard Gibbs free energy change ($\Delta G°$) (kJ mol^{-1}), standard entropy change ($\Delta S°$) (J mol^{-1} K^{-1}) and standard enthalpy change ($\Delta H°$) (kJ mol^{-1}) are calculated as follows [25]:

$$\Delta G° = -RT \ln K \tag{10}$$

$$\Delta G° = \Delta H° - \Delta S° \tag{11}$$

The van't Hoff equation is given as follows:

$$\ln K = \frac{-\Delta H°}{R} \times \frac{1}{T} + \frac{\Delta S°}{R} \tag{12}$$

where R is the gas constant (8.314 J mol^{-1} K^{-1}), K is the equilibrium constant calculated from the model that provides the best fit [26] and T is the temperature (K). The value of $\Delta G°$ can be calculated directly from Eq. (11) while $\Delta H°$ and $\Delta S°$ are determined from the slope and the intercept of a plot ln$K$ against 1/T respectively.

3. Results and discussion

3.1. Characterization of biochar

3.1.1. Physicochemical characterization of biochar

The carbon, hydrogen and nitrogen contents of biochar obtained from the elemental analysis are 50.32%, 2.32%, and 1.40% respectively. The specific surface area of biochar obtained by N_2 adsorption–desorption isotherm is 550 m^2 g^{-1} and this value is relatively large when compared with the other biochars like coconut shell (536 m^2 g^{-1}) [27], maize straw (70 m^2 g^{-1}) [28] and Eucalyptus sawdust (12.198 m^2 g^{-1}) [29]. In addition, biochar has an average pore diameter of 4.078 nm, hence according to the International Union of Pure and Applied Chemistry (IUPAC), the biochar can be considered as a mesoporous material [30].

3.1.2. XRD analysis of ALWSD and biochar

The XRD patterns are measured to analyze the crystalline phase of the ALWSD and its biochar. These patterns are shown in Fig. 1. The two peaks at approximately 2θ = 22° and 16° seen in ALWSD correspond to cellulose crystal structure and they become wider in biochar. This observation suggests that the structural destruction of cellulose occurs during pyrolysis and leads to the formation of amorphous structure in biochar. The amorphous structure is good evidence for dye adsorption purposes [31]. An amorphous adsorbent usually has an irregular surface with more empty sites and this allows the dye molecules to get entrapped into the adsorbent surface [32]. Some additional peaks are also observed in biochar structure indicating the presence of inorganic minerals such as calcite, quartz and sodium chloride [33].

3.1.3. FTIR analysis

The presence of functional groups on the biochar is confirmed by FTIR analysis. The FTIR spectra of biochar are obtained before and after the adsorption of BR29 and RR2 and the results are shown in Fig. 2. The biochar spectrum before dye adsorption shows a band at 3,446 cm^{-1} indicating the –OH stretching vibrations of water, alcohols, carboxylic acid, and phenols. The band at 2,917 and 2,847 cm^{-1} is attributed to the asymmetric and symmetric –CH stretching vibrations of $–CH_2$ group. The band at 1,437 cm^{-1} corresponds to –OH bending vibrations of phenol while the band at 1,388 cm^{-1} represents –CH bending in alkanes or aryl groups. Further, the band observed at 1,627 cm^{-1} confirms the presence of –COO group in biochar. After the adsorption process, the

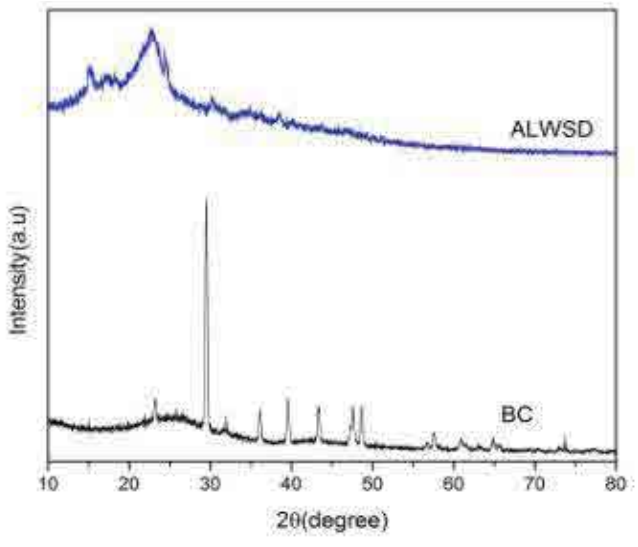

Fig. 1. XRD patterns of ALWSD and biochar.

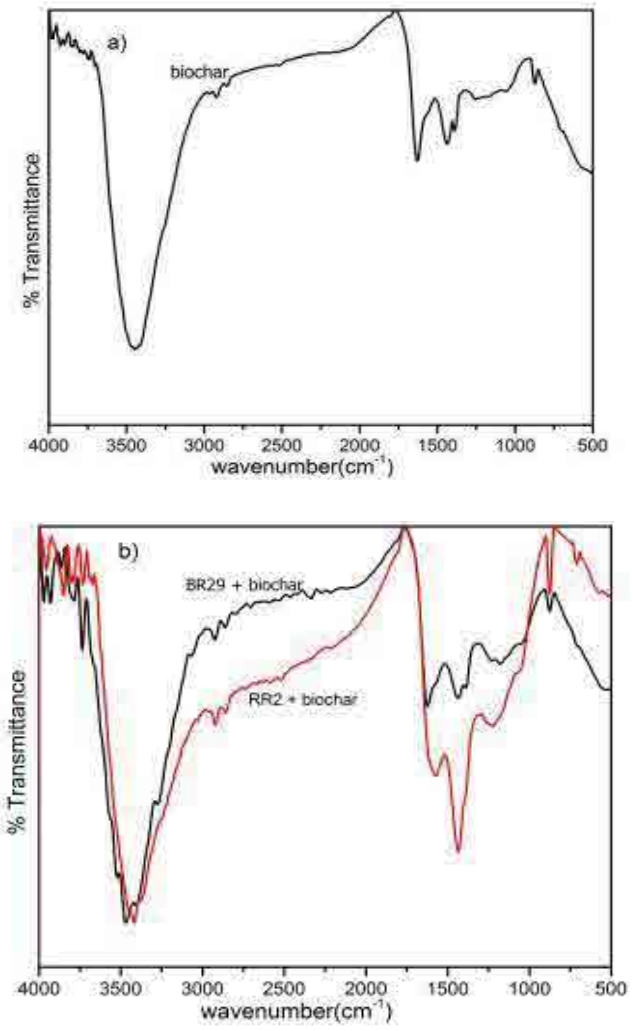

Fig. 2. FTIR spectra for biochar (a) before and (b) after adsorption of BR29 and RR2.

dye loaded biochar spectrum shows some changes in the above-mentioned bands. The band observed at 3,446; 2,917; 2,847; 1,627 and 1,437 cm^{-1} in the biochar before dye adsorption shifted to lower frequencies indicates the involvement of functional groups in the adsorption process. In addition, some new peaks observed at 1,179; 1,574; and 1,213 cm^{-1} in the dye loaded adsorbent confirm that the dye molecules are adsorbed on the surface of biochar.

3.1.4. FE-SEM analysis

Scanning electron microscopy (SEM) micrographs of biochar before and after adsorption are taken to analyze the changes in the surface morphology of the material as shown in Figs. 3a–c. The SEM image of biochar displays the pores present in the biochar before adsorption in Fig. 3a. It can be seen from Fig. 3b that there are no noticeable changes in the surface morphology of the biochar after being subjected to BR29 adsorption. However, the surface of biochar after being exposed to RR2 dye appears smooth and the pores are partially covered by the dye as seen in Fig. 3c.

3.2. Adsorption studies

3.2.1. Effect of contact time and initial dye concentration

Fig. 4 shows the adsorption capacity of biochar towards the percentage of BR29 and RR2 dye removal vs. contact time at the initial dye concentration of 40–100 mg L^{-1}. It can be seen that the performance increases with time until equilibrium is attained. This behavior is in good agreement with the previous studies reported for anionic and cationic dye removal [34,35]. The adsorption process attains equilibrium time within 10 min for BR29 and 70 min for RR2 and after that, there is no change in the removal percentage. This may be due to the saturation of reactive sites with dye molecules. The findings also reveal that BR29 dye reacts with the reactive sites of the biochar faster than RR2 and hence equilibrium is attained shortly.

3.2.2. Effect of pH

Fig. 5 shows the influence of pH on the adsorption efficiency of biochar. It can be seen that pH plays an important role in the adsorption process of both the dyes. It is observed from Fig. 5 that higher pH leads to the maximum removal percentage of BR29 while the decrease in pH favors the removal of RR2. This behavior is more common for cationic and anionic dyes reported in the literature [36,37] and can be explained by considering the electrokinetic behavior of the adsorbent. The high availability of ions like H^+ at acidic and OH^- in the basic solution may be the reason for decreasing the removal percentage of BR29 and RR2 in acidic and basic conditions respectively. pH_{ZPC} of an adsorbent is another reason to describe the adsorption behavior of anionic and cationic dyes. The pH_{ZPC} of the biochar is 7.5. This implies that when the pH of the dye solution is above pH_{ZPC}, the adsorbent surface would be negatively charged and it favors the adsorption of BR29 while below pH_{ZPC}, the adsorbent surface becomes positively charged, and hence it favors the adsorption of RR2 due to electrostatic attraction.

3.2.3. Effect of agitation speed

The agitation speed experiments are studied in the range of 30, 60, 90, 120, 150, and 170 rpm as shown in Fig. 6 keeping the other process parameters constant. It is observed that when the agitation speed increases from 30–170 rpm, the adsorption of both the dyes increases. Hence, the optimum agitation speed for both dyes is fixed at 170 rpm with the removal of 91.36% for BR29 and 79.83% for RR2. Lower agitation speed may cause inefficient diffusion of adsorbent in a solution that led to particle aggregation. The same findings are observed for the adsorption of crystal violet onto pineapple leaf powder [38] and acid orange 74 dye onto *Pinus roxburghii* leaves [39].

3.2.4. Effect of adsorbent dose

The effect of biochar dose on dye removal efficiency is investigated by varying the dosage of biochar from 25 to 200 mg at a fixed temperature, contact time and adsorbate concentration as shown in Fig. 7. It is observed from Fig. 7 that the dye uptake gets increased with an increased amount of

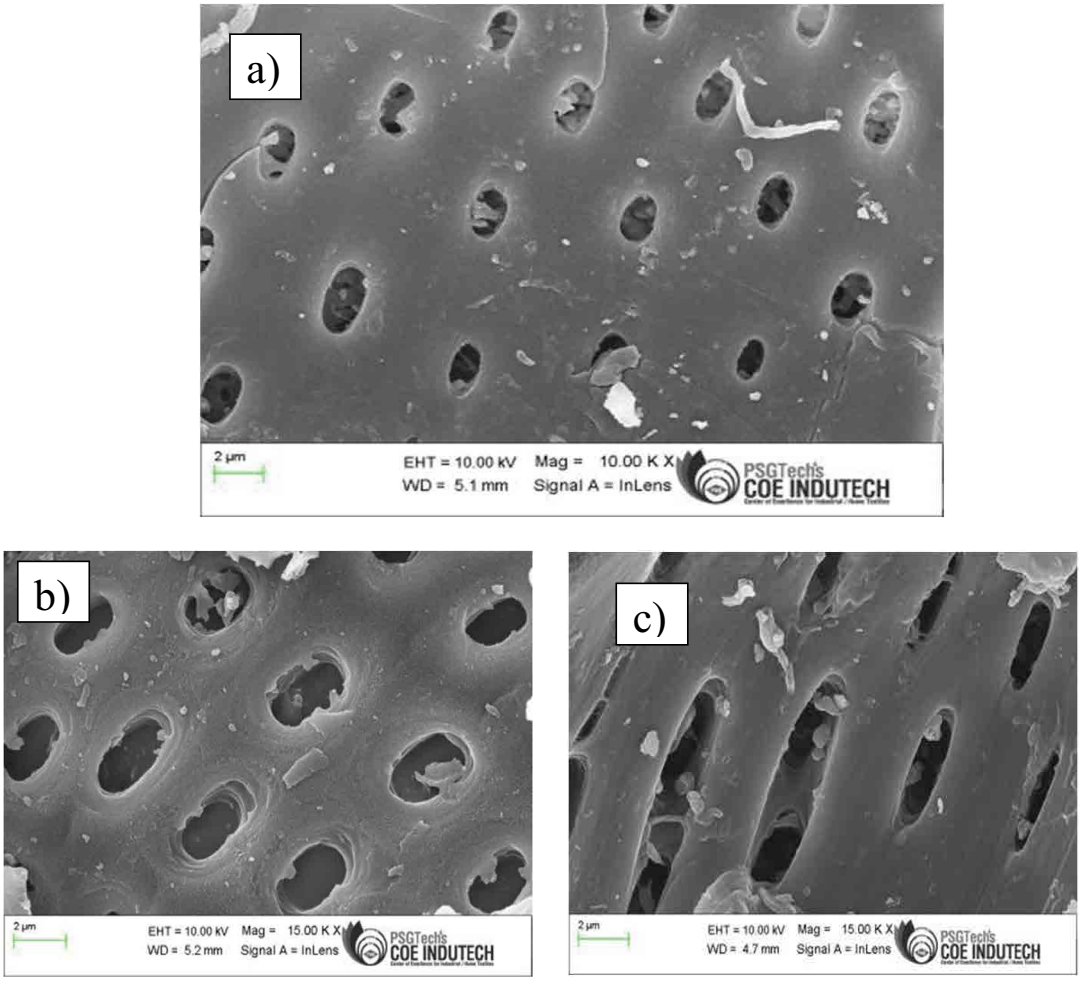

Fig. 3. SEM micrograph of biochar (a) before adsorption, (b) after the adsorption of BR29, and (c) after the adsorption of RR2.

biochar dose from 25 to 200 mg. However, the removal efficiency of 95% for BR29 and 90% for RR2 is achieved for 50 mg dose. Hence, for further studies, the optimum dose of 50mg is fixed for both the dyes.

3.2.5. Effect of temperature

The adsorption of BR29 and RR2 onto biochar is studied in the range of 300–320 K and shown in Fig. 8. It is observed from Fig. 8 that for both the dyes the amount of dye adsorbed increases with increasing temperature confirming the endothermic nature of the adsorption process. This may be the result of the increase in the number of adsorption sites in the adsorbent which is formed by breaking internal bonds in the adsorbent at high temperature [40]. The same trend is observed for the adsorption of BR29 by activated carbon and conducting polymer composites [41] and adsorption of Reactive Red 195 by *Euphorbia tirucalli* polypyrrole composite [42].

3.3. Adsorption kinetics

The adsorption kinetic curves of RR2 and BR29 onto the biochar at initial dye concentrations of 40, 60, 80, and 100 mg L^{-1} are shown in Fig. 9. The initial fast adsorption rate is achieved and then the equilibrium is attained. This trend commonly occurs when a fresh adsorbent with many active sites is in contact with the dye molecules. As time progresses, the number of free adsorption sites decreases and after that, there is no further adsorption. The same behavior is reported in the literature for anionic and cationic dyes [43].

To better understand the kinetic mechanism, kinetic models such as pseudo-first-order as in Eq. (4) and pseudo-second-order as in Eq. (5) are fitted with the experimental data and the results are summarized in Table 1. The high value of R^2 ($R^2 > 0.98$) for both the dyes indicates that the pseudo-second-order model is more suitable to describe the adsorption kinetics. Moreover, it is found that for all the studied concentrations, the calculated q_e values are close to the experimental q_e values. This confirms the better fit of the pseudo-second-order model. Similar results are reported for the adsorption kinetics of various pollutants onto activated carbons [44] and magnetic carbon nanotube [45]. Based on the assumptions of the pseudo-second-order model, it can be concluded that the adsorption of RR2 and BR29 onto biochar may follow chemisorption.

According to the Weber and Morris [22] linear intra-particle diffusion model, the plot of q vs $t^{0.5}$ should give a straight

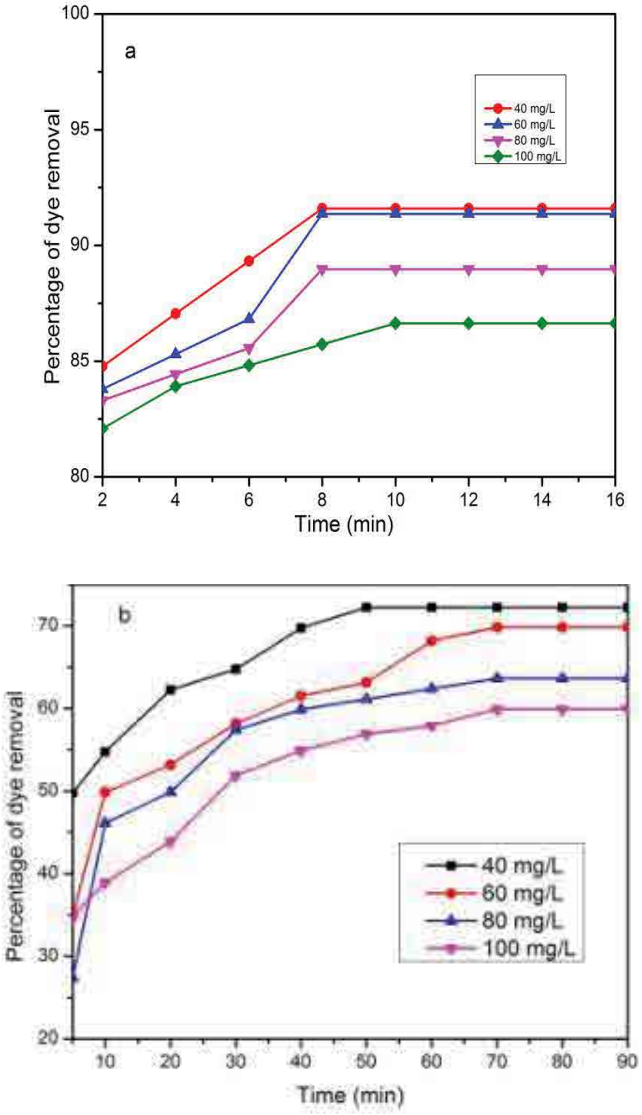

Fig. 4. Effect of contact time on the percentage removal of (a) BR29 and (b) RR2 at different initial dye concentrations.

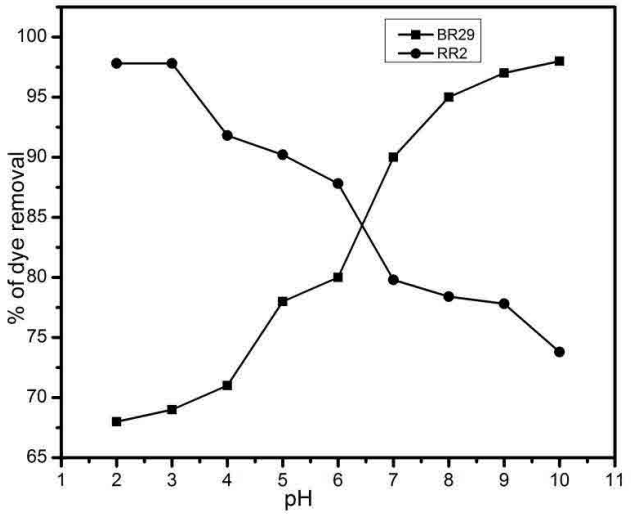

Fig. 5. Influence of pH on the percentage of BR29 and RR2 dye removal using biochar as adsorbent.

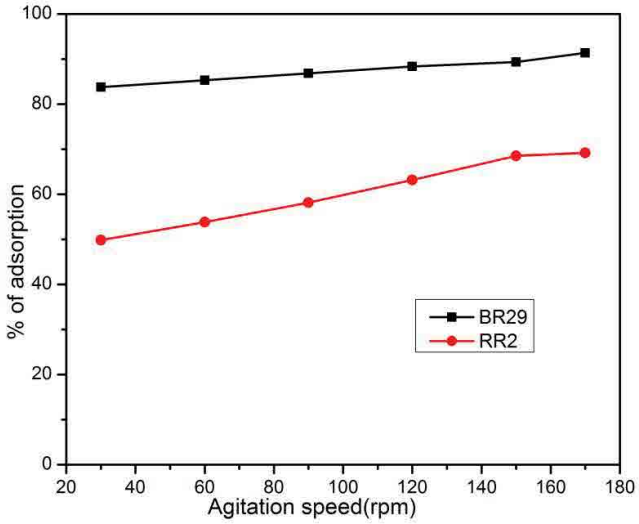

Fig. 6. Effect of agitation speed on BR29 and RR2 dye adsorption by biochar (biochar dose = 50 mg, dye concentration = 60 mg L^{-1} and temperature = 300 K).

line. If the straight line passes through the origin then the rate-limiting step is the intra-particle diffusion, otherwise, the adsorption process is controlled by some other mechanism. The parameters for the intra-particle diffusion model are presented in Table 1 and the linear plots are shown in Fig. 10. As the intercepts of all the plots are non zero, the intra-particle diffusion mechanism is not the rate-limiting step.

3.4. Adsorption isotherms

The adsorption isotherm in the present study is obtained at 300, 310, and 320 K with different initial dye concentrations (10–100 mg L^{-1}) at the equilibrium time of 10 min for BR29 and 70 min for RR2. Freundlich, Langmuir and Temkin isotherm models are used to analyze the equilibrium data. The parameter values for the adsorption of BR29 and RR2 onto the biochar calculated are summarized in Table 2. Based on R^2 value, the Freundlich model is selected as the best fit to represent the adsorption behavior of both the dyes on the biochar and the isotherm curves are shown in Fig. 11. This result is consistent with literature [46–48]. The K_F constant is found to decrease with the increase in temperature for RR2 confirming the exothermic nature of the adsorption process. Nevertheless, for BR29, the K_F value increases with the increasing temperature indicating that the adsorption process is endothermic. Moreover, the value of n greater than unity for both the dyes indicates favorable adsorption of anionic and cationic dyes on to the biochar. To evaluate the adsorption property of the biochar prepared, a comparison with the other adsorbents towards the removal of anionic and cationic dyes is made and the results are given in Table 3.

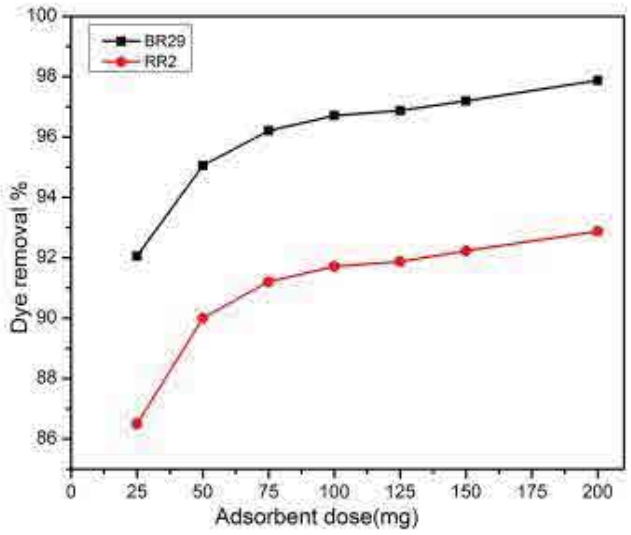

Fig. 7. Effect of adsorbent dose on the removal of BR29 and RR2 by biochar (dye concentration = 60 mg L^{-1} and temperature = 300 K).

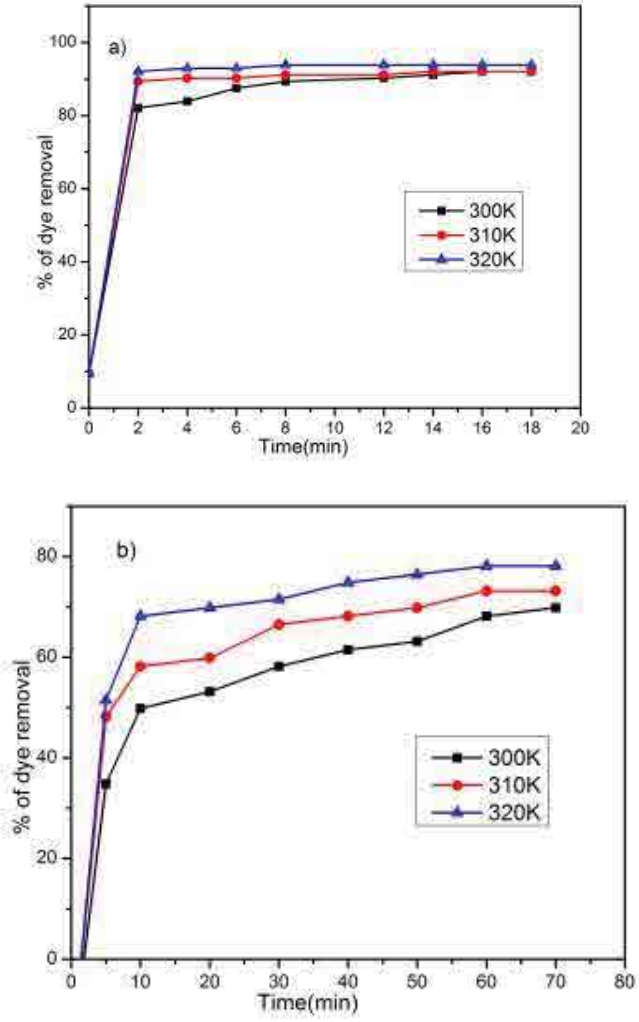

Fig. 8. Effect of temperature on the percentage of removal of (a) BR29 and (b) RR2 by biochar.

3.5. Adsorption thermodynamics

The thermodynamic parameters calculated for the adsorption process are shown in Table 4. The negative value of Gibbs free energy for BR29 and RR2 indicates that the adsorption of these dyes onto biochar occurs spontaneously [54]. The positive and negative values of $\Delta H°$ for BR29 and RR2 confirm the endothermic and exothermic nature of the adsorption process respectively. Moreover, the magnitude of $\Delta H°$ implies physisorption that occurs in the adsorption process. The positive $\Delta S°$ values indicate the good affinity between the adsorbent and the adsorbate during the adsorption process.

3.6. Proposed adsorption mechanism

Generally, the possible mechanism of dye adsorption is essential to understand the interaction of dyes and adsorbent. In the present study, electrostatic attraction can be considered to explain adsorbent-dye interaction in the dye adsorption mechanism. This interaction can be illustrated by

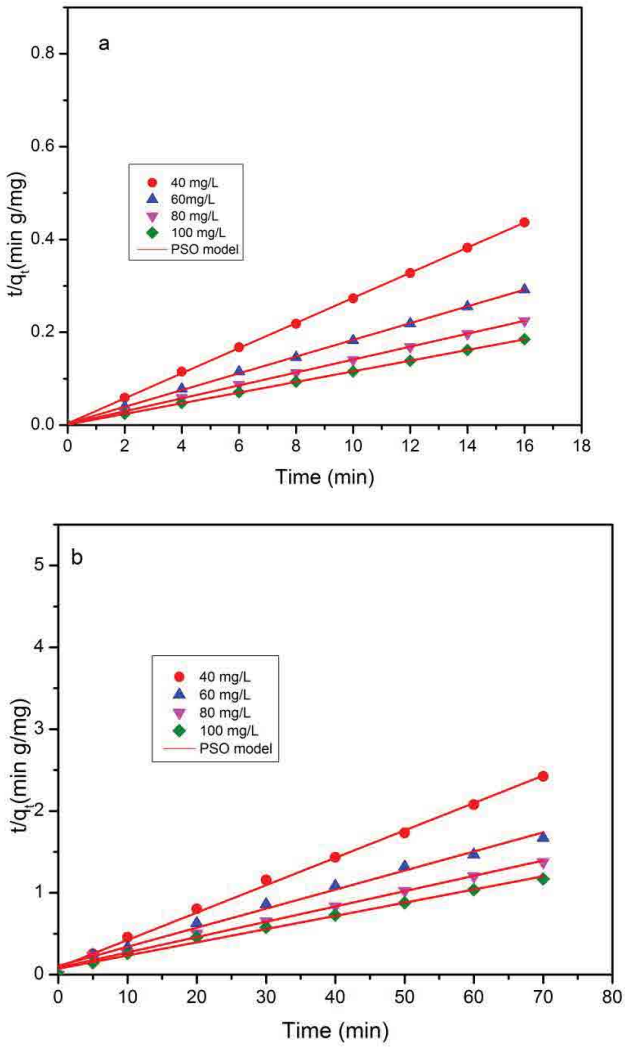

Fig. 9. Linear plots of pseudo-second-order kinetics for the adsorption of (a) BR29 and (b) RR2 dye adsorption onto biochar.

Table 1
Calculated kinetic parameters for BR29 and RR2 dye removal by the biochar at 300 K

Dyes	C_0 (mg L^{-1})	q_{exp} (mg g^{-1})	Pseudo-first-order			Pseudo-second-order			Intraparticle diffusion		
			q_{cal} (mg g^{-1})	k_1 (min^{-1})	R^2	q_{cal} (mg g^{-1})	k_2 (g mg^{-1} min^{-1})	R^2	k_p (mg g^{-1} $min^{-1/2}$)	C (mg g^{-1})	R^2
BR29	40	36.64	5.56	0.5596	0.6993	36.95	0.2092	0.9997	8.44	9.84	0.5851
	60	54.82	14.56	0.6829	0.6806	55.46	0.0982	0.9994	10.32	21.69	0.6243
	80	71.18	88.03	0.4941	0.5976	71.83	0.1003	0.9996	14.11	26.23	0.5930
	100	86.64	27.47	0.6382	0.7992	87.18	0.1154	0.9999	15.85	36.32	0.5762
RR2	40	34.9	19.77	0.0213	0.7018	29.86	0.0128	0.9965	3.35	5.73	0.6998
	60	41.9	32.42	0.0514	0.8857	42.93	0.0050	0.9884	5.41	2.25	0.7722
	80	50.9	1.21	0.0431	0.9923	53.41	0.0041	0.9922	7.02	1.24	0.78
	100	59.9	43.74	0.0533	0.9574	61.99	0.0036	0.9902	7.10	7.92	0.8108

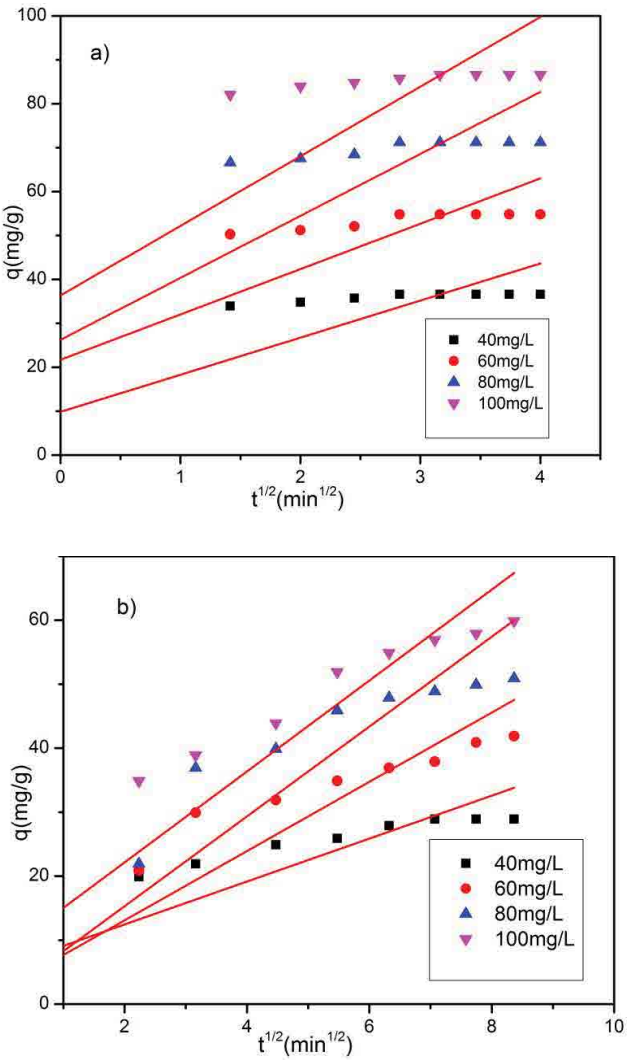

Fig. 10. Linear plots of the intra-particle diffusion model for the removal of (a) BR29 and (b) RR2 onto biochar.

considering the point of zero charges (pH_{ZPC}) of adsorbent and the pH dependence of the adsorption of biochar onto BR29 and RR2. Fig. 12 gives the representation of the proposed adsorption mechanisms of dye molecules by the BC. The pH_{ZPC} of the biochar is 7.5 and it can be observed that the biochar adsorption capacity reaches a maximum at pH 2 for RR2 and pH 10 for BR29. At low pH, the adsorbent surface gets a positive charge ($pH < pH_{ZPC}$), hence it favors the adsorption of anionic dyes, but at higher pH, the adsorbent surface gets a negative charge ($pH > pH_{ZPC}$), hence it favors the adsorption of cationic dye. Based on the above discussion the following mechanism is proposed to explain the possible electrostatic interactions of dyes and adsorbent.

4. Conclusion

In the present study, the removal of cationic dye BR29 and anionic dye RR2 from aqueous solutions is investigated using ALWSD derived biochar as a low-cost adsorbent. The biochar exhibits a specific surface area of 550 m^2 g^{-1}. Equilibrium time

Table 2
Isotherm parameters of BR29 and RR2 dye sorption calculated from the Langmuir, Freundlich, and Temkin models

Dyes	Temperature (K)	Parameters								
		Langmuir isotherm			Freundlich isotherm			Temkin isotherm		
		Q^0_{max} (mg g^{-1})	K_L (L mg^{-1})	R^2	K_f (mg g^{-1})(L mg^{-1})$^{-1/n}$	n	R^2	B (J mol^{-1})	K_T (L mg^{-1})	R^2
Basic Red 29	300	158	0.084	0.9358	13.41	1.35	0.9921	112.55	8.4	0.8449
	310	126	0.162	0.8622	13.78	1.36	0.9919	113.91	8.1	0.8456
	320	163	0.189	0.6219	14.07	1.36	0.9945	115.89	8.5	0.8387
Reactive Red 2	300	232	0.08	0.6775	23.09	2.15	0.9448	123.37	0.66	0.8416
	310	227	0.05	0.6261	22.28	2.15	0.9455	183.21	6.7	0.6058
	320	121	0.06	0.7757	20.56	2.72	0.9725	163.67	8.5	0.7298

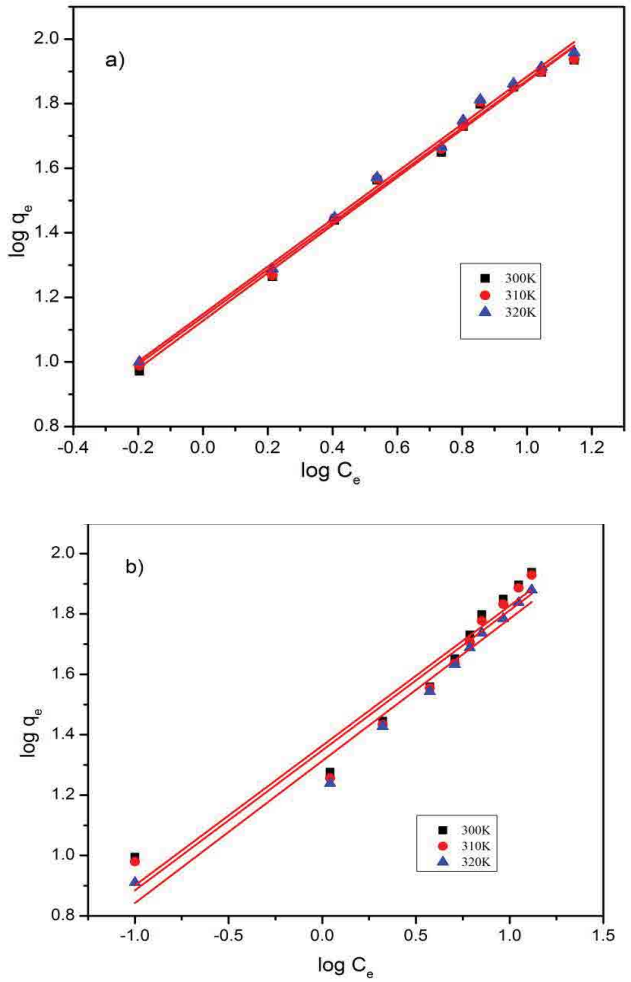

Fig. 11. Linear plots of Freundlich isotherm curves for the adsorption of (a) BR29 and (b) RR2 onto biochar.

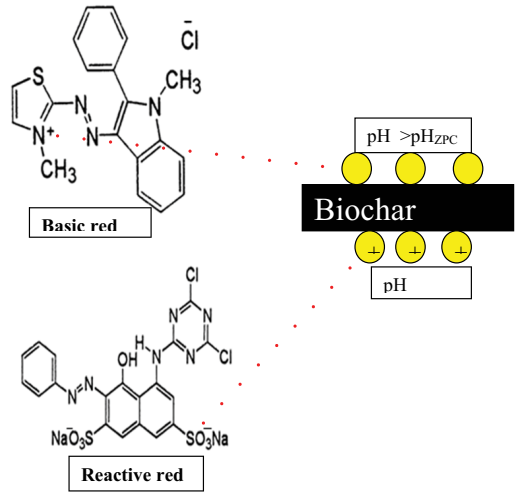

Fig. 12. The proposed mechanism to explain the possible electrostatic interactions of dyes and adsorbent.

Table 3
Comparison of the adsorption capacities of various adsorbents used for anionic and cationic dye removal

Materials	Dye	Temperature (°C)	Maximum adsorption capacity q_m (mg g^{-1})	References
Coffee residues	Basic Blue 3G	25	179	[49]
Pine tree leaves	Basic Red 46	45	71.94	[50]
Pine cone	Basic Red 46	45	73.53	[51]
Peanut hull	Reactive Black 5	60	55.55	[52]
Biochar	Reactive Red 141	35	130	[32]
Saw dust	Reactive Red 141	25	2.12	[53]
Acacia leucophloea wood sawdust biochar	Basic Red 29	27	158	This work
	Reactive Red 2		232	

Table 4
Thermodynamic parameters of BR29 and RR2 dye sorption process by the biochar

Dye	Temperature (K)	Equilibrium constant K	$\Delta G°$ (kJ mol^{-1})	$\Delta H°$ (kJ mol^{-1})	$\Delta S°$ (J mol^{-1} K^{-1})
BR29	300	13.41	–64.74	19.19	27.98
	310	13.78	–67.60		
	320	14.07	–70.34		
RR2	300	23.09	–78.30	–46.10	10.79
	310	22.28	–79.99		
	320	20.56	–80.43		

is attained within 20 min for BR29 and 70 min for RR, which is a short period. Kinetic study indicates that the adsorption of BR29 and RR2 onto biochar follows pseudo-second-order kinetics. Likewise, the adsorption isotherm study shows that the equilibrium data are well explained by the Freundlich isotherm model. Based on the results obtained, it is noted that the biochar could be used as an efficient adsorbent for the removal of cationic and anionic dyes from aqueous solutions.

References

[1] N. Bensalah, M.A. Quiroz Alfaro, C.A. Martinez-Huitle, Electrochemical treatment of synthetic wastewaters containing Alphazurine A dye, Chem. Eng. J., 149 (2009) 348–352.

[2] S. Dawood, T.K. Sen, C. Phan, Synthesis and characterisation of novel-activated carbon from waste biomass pine cone and its application in the removal of Congo red dye from aqueous solution by adsorption, Water Air Soil Pollut., 225 (2014) 1–16.

[3] M.T. Yagub, T.K. Sen, S. Afroze, H.M. Ang, Dye and its removal from aqueous solution by adsorption: a review, Adv. Colloid Interface Sci., 209 (2014) 172–184.

[4] D. Karadag, E. Akgul, S. Tok, F. Erturk, M.A. Kaya, M. Turan, Basic and reactive dye removal using natural and modified zeolites, J. Chem. Eng. Data, 52 (2007) 2436–2441.

[5] M. Asgher, H.N. Bhatti, Evaluation of thermodynamics and effect of chemical treatments on sorption potential of *Citrus* waste biomass for removal of anionic dyes from aqueous solutions, Ecol. Eng., 38 (2012) 79–85.

[6] M.T. Yagub, T.K. Sen, H.M. Ang, Equilibrium, kinetics, and thermodynamics of methylene blue adsorption by pine tree leaves, Water Air Soil Pollut., 223 (2012) 5267–5282.

[7] L.D.T. Prola, E. Acayanka, E.C. Lima, C.S. Umpierres, J.C.P. Vaghetti, W.O. Santos, S. Laminsi, P.T. Djifon, Comparison of *Jatropha curcas* shells in natural form and treated by non-thermal plasma as biosorbents for removal of Reactive Red 120 textile dye from aqueous solution, Ind. Crops Prod., 46 (2013) 328–340.

[8] V.K. Gupta, Suhas, Application of low-cost adsorbents for dye removal – a review, J. Environ. Manage., 90 (2009) 2313–2342.

[9] O. Duman, S. Tunç, T.G. Polat, Determination of adsorptive properties of expanded vermiculite for the removal of C.I. Basic Red 9 from aqueous solution: kinetic, isotherm and thermodynamic studies, Appl. Clay Sci., 109–110 (2015) 22–32.

[10] O. Duman, S. Tunç, T.G. Polat, Adsorptive removal of triarylmethane dye (Basic Red 9) from aqueous solution by sepiolite as effective and low-cost adsorbent, Microporous Mesoporous Mater., 210 (2015) 176–184.

[11] E. Ayranci, O. Duman, In-situ UV-visible spectroscopic study on the adsorption of some dyes onto activated carbon cloth, Sep. Sci. Technol., 44 (2009) 3735–3752.

[12] O. Duman, S. Tunç, B.K. Bozoğlan, T.G. Polat, Removal of triphenylmethane and reactive azo dyes from aqueous solution by magnetic carbon nanotube-κ-carrageenan-Fe_3O_4 nanocomposite, J. Alloys Compd., 687 (2016) 370–383.

[13] O. Duman, S. Tunç, T.G. Polat, B.K. Bozoğlan, Synthesis of magnetic oxidized multiwalled carbon nanotube-κ-carrageenan-Fe_3O_4 nanocomposite adsorbent and its application in cationic Methylene Blue dye adsorption, Carbohydr. Polym., 147 (2016) 79–88.

[14] D. Klinar, Universal model of slow pyrolysis technology producing biochar and heat from standard biomass needed for the techno-economic assessment, Bioresour. Technol., 206 (2016) 112–120.

[15] D. Mohan, A. Sarswat, Y.S. Ok, C.U. Pittman Jr., Organic and inorganic contaminants removal from water with biochar, a renewable, low cost and sustainable adsorbent – a critical review, Bioresour. Technol., 160 (2014) 191–202.

[16] L.J. Leng, X.Z. Yuan, H.J. Huang, J.G. Shao, H. Wang, X.H. Chen, G.M. Zeng, Bio-char derived from sewage sludge by liquefaction: characterization and application for dye adsorption, Appl. Surf. Sci., 346 (2015) 223–231.

[17] J. Georgin, G.L. Dotto, M.A. Mazutti, E.L. Foletto, Preparation of activated carbon from peanut shell by conventional pyrolysis and microwave irradiation-pyrolysis to remove organic dyes from aqueous solutions, J. Environ. Chem. Eng., 4 (2016) 266–275.
[18] H. Li, S.A.A. Mahyoub, W. Liao, S. Xia, H. Zhao, M. Guo, P. Ma, Effect of pyrolysis temperature on characteristics and aromatic contaminants adsorption behavior of magnetic biochar derived from pyrolysis oil distillation residue, Bioresour. Technol., 223 (2017) 20–26.
[19] T. Zehra, N. Priyantha, L.B.L. Lim, E. Iqbal, Sorption characteristics of peat of Brunei Darussalam V: removal of Congo red dye from aqueous solution by peat, Desal. Wat. Treat., 54 (2015) 2592–2600.
[20] S. Lagergren, About the theory of so-called adsorption of soluble substances, Kungliga Svenska Vetenskapsakademiens Handlingar, 24 (1898) 1–39.
[21] Y.S. Ho, G. Mckay, Kinetic models for the sorption of dye from aqueous solution by wood, Process Saf. Environ. Prot., 76 (1998) 183–191.
[22] W.J. Weber, J.C. Morris, Kinetics of adsorption on carbon from solution, J. Sanitary Eng. Div., ASCE, 89 (1963) 31–60.
[23] I. Langmuir, The adsorption of gases on plane surfaces of glass, mica and platinum, J. Am. Chem. Soc., 40 (1918) 1361–1403.
[24] H.M.F. Freundlich, Over the adsorption in solution, J. Phys. Chem. A, 57 (1906) 358–471.
[25] Mu. Naushad, S. Vasudevan, G. Sharma, A. Kumar, Z.A. ALOthman, Adsorption kinetics, isotherms, and thermodynamic studies for Hg^{2+} adsorption from aqueous medium using alizarin red-S-loaded amberlite IRA-400 resin, Desal. Wat. Treat., 57 (2016) 18551–18559.
[26] S. Chowdhury, R. Mishra, P. Saha, P. Kushwaha, Adsorption thermodynamics, kinetics and isosteric heat of adsorption of malachite green onto chemically modified rice husk, Desalination, 265 (2011) 159–168
[27] Y. Liu, Is the free energy change of adsorption correctly calculated?, J. Chem. Eng. Data, 54 (2009) 1981–1985.
[28] H.N. Tran, S.-J. You, H.-P. Chao, Y.-F. Wang, Sustainable Biochar Derived from Agricultural Wastes for Removal of Methylene Green 5 from Aqueous Solution: Adsorption Kinetics, Isotherms, Thermodynamics, and Mechanism Analysis, Chapter 12, T.K. Sen, Ed., Air, Gas, and Water Pollution Control Using Industrial and Agricultural Solid Wastes Adsorbents, CRC Press, USA, 2017, p. 255.
[29] X.B. Wang, W. Zhou, G.Q. Liang, D. Song, X.Y. Zhang, Characteristics of maize biochar with different pyrolysis temperatures and its effects on organic carbon, nitrogen and enzymatic activities after addition to fluvo-aquic soil, Sci. Total Environ., 538 (2015) 137–144.
[30] X.J. Zhang, L. Zhang, A.M. Li, *Eucalyptus* sawdust derived biochar generated by combining the hydrothermal carbonization and low concentration KOH modification for hexavalent chromium removal, J. Environ. Manage., 206 (2018) 989–998.
[31] M. Thommes, K. Kaneko, A.V. Neimark, J.P. Olivier, F. Rodriguez-Reinoso, J. Rouquerol, K.S.W. Sing, Physisorption of gases, with special reference to the evaluation of surface area and pore size distribution (IUPAC technical report), Pure Appl. Chem., 87 (2015) 1051–1069.
[32] M.A. Zazycki, M. Godinho, D. Perondi, E.L. Foletto, G.C. Collazzo, G.L. Dotto, New biochar from pecan nutshells as an alternative adsorbent for removing reactive red 141 from aqueous solutions, J. Cleaner Prod., 171 (2018) 57–65.
[33] G. Crini, P.-M. Badot, Application of chitosan, a natural aminopolysaccharide, for dye removal from aqueous solutions by adsorption processes using batch studies: a review of recent literature, Prog. Polym. Sci., 33 (2008) 399–447.
[34] Q.L. Ma, W. Song, R.B. Wang, J. Zou, R.D. Yang, S.B. Zhang, Physicochemical properties of biochar derived from anaerobically digested dairy manure, Waste Manage., 79 (2018) 729–734.
[35] A.K. Kushwaha, N. Gupta, M.C. Chattopadhyaya, Removal of cationic methylene blue and malachite green dyes from aqueous solution by waste materials of *Daucus carota*, J. Saudi Chem. Soc., 18 (2014) 200–207.
[36] F. Deniz, S.D. Saygideger, Removal of a hazardous azo dye (Basic Red 46) from aqueous solution by princess tree leaf, Desalination, 268 (2011) 6–11.
[37] F. Deniz, S. Karaman, S.D. Saygideger, Biosorption of a model basic dye onto *Pinus brutia* Ten.: evaluating of equilibrium, kinetic and thermodynamic data, Desalination, 270 (2011) 199–205.
[38] F. Deniz, S. Karaman, Removal of an azo-metal complex textile dye from colored aqueous solutions using an agro-residue, Microchem. J., 99 (2011) 296–302.
[39] S. Neupane, S.T. Ramesh, R. Gandhimathi, P.V. Nidheesh, Pineapple leaf (*Ananas comosus*) powder as a biosorbent for the removal of crystal violet from aqueous solution, Desal. Wat. Treat., 54 (2014) 1–14.
[40] R. Rehman, S.J. Muhammad, M. Arshad, Brilliant green and acid Orange 74 dyes removal from water by *Pinus roxburghii* leaves in naturally benign way: an application of green chemistry, J. Chem., 2019 (2019) 10 p, https://doi.org/10.1155/2019/3573704.
[41] M. Jain, V.K. Garg, K. Kadirvelu, Adsorption of hexavalent chromium from aqueous medium onto carbonaceous adsorbents prepared from waste biomass, J. Environ. Manage., 91 (2010) 949–957.
[42] A. Geetha, N. Palanisamy, Equilibrium and kinetic studies for the adsorption of Basic Red 29 from aqueous solutions using activated carbon and conducting polymer composite, Desal. Wat. Treat., 57 (2015) 8406–8419.
[43] P.N. Palanisamy, A. Agalya, P. Sivakumar, Polymer composite—a potential biomaterial for the removal of reactive dye, E-J. Chem., 9 (2012) 1823–1834.
[44] A. Gücek, S. Şener, S. Bilgen, M.A. Mazmancı, Adsorption and kinetic studies of cationic and anionic dyes on pyrophyllite from aqueous solutions, J. Colloid Interface Sci., 286 (2005) 53–60.
[45] E. Ayranci, O. Duman, Removal of anionic surfactants from aqueous solutions by adsorption onto high area activated carbon cloth studied by in situ UV spectroscopy, J. Hazard. Mater., 148 (2007) 75–82.
[46] O. Duman, C. Özcan, T.G. Polat, S. Tunç, Carbon nanotube-based magnetic and non-magnetic adsorbents for the high-efficiency removal of diquat dibromide herbicide from water: OMWCNT, OMWCNT-Fe_3O_4 and OMWCNT-κ-carrageenan-Fe_3O_4 nanocomposites, Environ. Pollut., 244 (2019) 723–732.
[47] O. Duman, E. Ayranci, Adsorption characteristics of benzaldehyde, sulphanilic acid, and p-phenolsulfonate from water, acid, or base solutions onto activated carbon cloth, Sep. Sci. Technol., 41 (2006) 3673–3692.
[48] O. Duman, E. Ayranci, Structural and ionization effects on the adsorption behaviors of some anilinic compounds from aqueous solution onto high-area carbon-cloth, J. Hazard. Mater., 120 (2005) 173–181.
[49] G.Z. Kyzas, N.K. Lazaridis, A.Ch. Mitropoulos, Removal of dyes from aqueous solutions with untreated coffee residues as potential low-cost adsorbents: equilibrium, reuse and thermodynamic approach, Chem. Eng. J., 189–190 (2012) 148–159.
[50] F. Deniz, S. Karaman, Removal of Basic Red 46 dye from aqueous solution by pine tree leaves, Chem. Eng. J., 170 (2011) 67–74.
[51] F. Deniz, S. Karaman, S.D. Saygideger, Biosorption of a model basic dye onto *Pinus brutia* Ten.: evaluating of equilibrium, kinetic and thermodynamic data, Desalination, 270 (2011) 199–205.
[52] M.S. Tanyildizi, Modeling of adsorption isotherms and kinetics of reactive dye from aqueous solution by peanut hull, Chem. Eng. J., 168 (2011) 1234–1240.
[53] P. Srivatsa, B. Tanwar, S. Goyal, P.K. Patnala, A comparative study of sonosorption of Reactive Red 141 dye on TiO_2, banana peel, orange peel and hardwood saw dust, J. Appl. Chem., 1 (2012) 505–511.
[54] M.U. Dural, L. Cavas, S.K. Papageorgiou, F.K. Katsaros, Methylene blue adsorption on activated carbon prepared from *Posidonia oceanica* (L.) dead leaves: kinetics and equilibrium studies, Chem. Eng. J., 168 (2011) 77–85.